Letters in Applied NanoBioScience
Open-Access Journal (ISSN: 2284-6808)

Article
Volume 12, Issue 4, 2023, 164
https://doi.org/10.33263/LIANBS124.164

Investigation of Zn Substituted Ba-W-type Base Ferrites for FT-IR Structural and Vibrational Studies

A. H. AL-Hammadi [1], Sadiq.H. Khoreem [1,2,*], W. F.Al-ryani [3]

[1] Physics Department, Faculty of Science, Sana'a University, Sana'a, Yemen
[2] Dept. of Optometry and Vision Science, Faculty of Medical Sciences, Al-Razi University, Sana'a, Yemen
[3] Physics Department, Faculty of Science, Saada University, Saada, Yemen
* Correspondence: khoreems@yahoo.com (S.H.K.);

Scopus Author ID 57571836200
Received: 27.11.2021; Accepted: 12.12.2021; Published: 21.11.2022

Abstract: Polycrystalline of $BaNi_{x-2}Zn_xFe_{16}O_{27}$ (where x = 0.0,0.4,0.8,1.2,1.6, and 2.0), hexagonal ferrites samples were synthesized by using the conventional standard ceramic method. Fourier Infrared (F.I.T.R.) Spectroscopy analysis was used to investigate the structural parameters of the samples. FT-IR spectra of the samples have been analyzed in the frequency range (400-4000) cm^{-1}. The result shows that the two main bands of absorption corresponding to tetrahedral v_1 and octahedral v_2 were observed, illustrating the ferrite phase formation. The high-frequency band in the range 550-600 cm^{-1} and a low-frequency band at around 400 cm^{-1} were assigned to tetrahedral v_1 and octahedral v_2 sites, respectively. The force constants (F_C) were calculated for tetrahedral F_{tet} sites and octahedral F_{oct} sites and were found to decrease with increasing Zn ions. Debye temperature (θ_D) also has been estimated as a function of composition at room temperature using FTIR spectra.

Keywords: W-type hexa-ferrites; Fourier transforms infrared; Debye temperature; force constants.

1. Introduction

Investigation of ferrite nanoparticles recently became much more interesting due to improving their electrical and magnetic properties, also interesting due to their excellent physical properties. The w-type Hexa-ferrites have been wide- various fields of science, industrial, and technological applications, including humidity sensors, recording disks, microwave devices, catalysts, Information storage, Magnetic Resonance Imaging, ceramic coatings for solar cells, optoelectronic devices, and electronic devices. [1,2]. The optical properties of the dielectric materials generally became of interest because of their Sensible transmission within the optical part of the spectrum as compared with different categories of materials. So, to study the optical properties of ferrite materials, the optical constants such as absorption coefficient, transmission, reflection, and index of refraction are vital parameters to explain the optical properties of ferrite materials [3]. The reportable by Narang *et al*. about the Ni-Zn ferrites was different by substituting Zn^{2+} ions that prefer tetrahedral sites, with divalent metal ions that either adopt octahedral positions or inhibit grain growth and the magnetic properties tailored with careful addition [4]. Shaukat, S. F. *et al*. reported the Cr-substituted W-type hexaferrite with the chemical formula ($BaNi_2Cr_xFe_{16-x}O_{27}$. IR spectrum for sintered sample revealed two well-defined absorption peaks, which correspond to tetrahedral A- and octahedral B-sites present in W-type hexagonal lattice [5]. Batoo, Khalid Muajsam, *et al*. reported the synthesis of Ba-doped Co–Zn ferrite nanoparticles using the sol-gel auto-

combustion technique. The single-phase formation of the samples with F*d*3m space group was confirmed by X-ray diffraction (XRD). Fourier transformation infrared (FTIR) spectra show the presence of two strong peaks around 430 cm^{-1} and 580 cm^{-1} that confirmed the formation of ferrite structure [6]. The general behavior for the nickel ferrites prefers to occupy the octahedral sites, while the zinc prefers to occupy the tetrahedral site. The interactions between the tetrahedral ions and octahedral sites will alter ferrites' electrical and magnetic properties. The octahedral sites are occupied by Ni^{2+} and $Fe^{3+,}$ whereas Zn2+ and Fe3+ occupy the tetrahedral sites. The properties of the ferrite are also strongly dependent on the synthesis method, sintering temperature, chemical composition, etc. [7–9]. The infrared spectroscopy method is based on the observation that a chemical compound exhibits pronounced selective infrared absorption. Different bands in the IR spectra represent the characteristic functional groups and bonds found in the chemical compound. To ascertain local symmetry, analyze noncrystalline solids, and research ordering phenomena in ferrite, infrared spectra are helpful. In the present study, we investigated and discussed the Fourier transformation infrared (FT-IR) spectra of the $BaNi_{x-2}Zn_xFe_{16}O_{27}$ Hexagonal ferrites, where x = 0.0, 0.4 0.8, 1.2, 1.6 and 2) 1.0 in the step of 0.20, which have been synthesis by the ceramic method.

2. Materials and Methods

The Zn substituted $BaNi_{2-x}Zn_xF_{16}O_{27}$ ferrites were prepared by Conventional Ceramic. The samples used in this work were prepared by the well-known ceramic method. In this method, high purity of $BaCo_3$, ZnO, NiO, and $Fe2O_3$, with purity >99 %, were mixed according to their molecular weight ratio to obtain different compositions of the relation. Different compositions follow the relation.

$$BaCo_3+(2-x)(NiO)+x(ZnO)+8Fe_2O_3 \text{-»} BaNi_{(2-x).}Zn_xFe_{16}O_{27}+CO_2\uparrow$$

where x = 0.0, 0.4, 0.8, 1.2, 1.6, and 2.

The weights of the mixed oxides in grams for each composition of the prepared system $BaNi_{2-x}Zn_xFe_{16}O_{27}$. For each sample, the oxides were combined and finely ground for an hour in a carborundum agate mortar, and then each sample was grounded again for five hours using a mechanical grinding machine. The mixture powder was pre-sintered in the air at 950 °C± 10°C for 6 hours and then slowly cooled to room temperature. The mixture was grounded again for five hours for each sample using the mechanical grinding machine to get a very fine powder. It was finally sintered for 4 hours at 1250°C plus 10°C before slowly cooling to ambient temperature. According to Stimson and Schiedt's method, the samples were created by combining 2.5 mg of ferrite with 0.8 g of KBr powder and pressing them into a 20 mm diameter cylindrical die and then pressed for about 15 min at 15 Pascal. C1ear disks of approximately 1 mm thickness were obtained with the usable transmission. FT-IR spectra of finely fine powder of all the compositions were recorded in the range of 4000 to 400 cm^{-1}, and measurements were made at room temperature.

3. Results and Discussion

The formation of the surface functional group was confirmed by IR spectroscopy. To detect the metaloxygen bond of the formed hexagonal $BaNi_{x-2}Zn_xFe_{16}O_{27}$ phase materials, A few milligrams of $BaNi_{x-2}Zn_xFe_{16}O_{27}$ powder mixed with anhydrous KBr powder and made in the form of a pellet for measurement. The FT-IR spectra were analyzed in the wavenumber

range between 4000 and 400 cm^{-1} for the samples shown in Figure 1. Generally, all of the samples have the metal-oxygen (M-O) and carbon-oxygen (C-O) bonds, as shown in Figure 1 and Table 1. This demonstrates a link between the oxygen in the specimen and the metals Fe, Ba, Ni, and Zn. The sample exhibits absorption bands appearing from the ferrite compounds appear. Generally, two significant peaks can be observed at (430 - 439.69 &580 - 595 cm^{-1}) are observed. The peaks appearing between 400 and 600 cm^{-1} are the result of the vibration of the metal-oxygen bond, which gives the idea of the formation of the ferrite phase[10]. These two distinct bands are attributed to the intrinsic vibrations of the tetrahedral and octahedral metal-oxygen band in the crystal lattices of the $BaNi_{x-2}Zn_xFe_{16}O_{27}$ hexagonal ferrite, respectively high-frequency and low-frequency band [11-13]. These two prominent peaks indicate the formation of hexaferrite. The stretching vibrations of the metal-oxygen bond are the reason for these peaks. The absorption peak at 1430 cm^{-1} is due to C–O asymmetric stretching vibration in the $BaCO_3$. The absorption bands around 1624cm^{-1} and 3449cm^{-1}peaks are due to O-H stretching vibrations of water mode. The H–O–H and O–H stretching vibration at wavenumbers around 3342 cm^{-1} and 1664 cm^{-1} due to the water and polyol in the precursor [14,15]. Bands located at 3435 cm^{-1} and 1590 cm^{-1} are due to the presence of O-H stretching vibration of (O–H) group of residual water and anti-symmetrical stretching vibration of CO_2, respectively [16]. Also are assigned to stretching and bending vibration of H_2O absorbed from the atmosphere when the samples were kept and ground in the air due to the high surface area of these materials [17]. The peak at 2348 cm^{-1} occurs due to the presence of CO_2 in the prepared sample [18]. The absorption band at 2900 cm^{-1} is assigned to the C–H stretching vibration [19]. Because Zn^{2+} has a lower atomic weight than its host Ni^{2+} and because the wavenumber is inversely related to the atomic weight, the band locations ν_1–ν_2 marginally rise when x increases [20].

3.1. Force constants.

Figure 2.a displays the variation in wavenumbers (ν_1& ν_2) with zinc concentration (x) for all samples. As can be seen from the figure, a large ionic radius of Zn^{2+} ion samples is expected to produce the ν_2 shift towards lower frequencies, whereas the ν_1 shift towards higher frequencies is expected with zinc concentration (x) [21]. The relation [22,23] is used to compute the values of the force constants (F_{tet} and F_{oct}) for the band Fe^{3+} - O^{2-} at tetrahedral and octahedral sites.

$$F_{tet} = 4\,\pi^2 c^2 \nu_1^2 \mu \qquad (1)$$

$$F_{oct} = 4\pi^2 c^2 \nu_2^2 \mu \qquad (2)$$

where c=2.99x1010 cm/s is the speed of light, Ftet is the tetrahedral force constant, Foct is the octahedral force constant, and 1 and 2 are the band wavenumbers in cm-1 and is the decreased mass for Fe^{3+} ions and O^{2-} ions, respectively (2.061x10-23 g).

Table 1 lists the values of the force constants for the tetrahedral (Ftet) and octahedral (Foct) sites. Figure 2.b displays the variation in the force constant with zinc concentration(x) for all samples at the tetrahedral and octahedral locations. It can be seen from the figure that Ftet decreases as zinc concentration rises. The fluctuation in cation oxygen bond length is responsible for this behavior [24]. The energy needed to break longer bonds is lower since the bond length (A-O) rose as zinc concentration increased, suggesting a drop in the force constant of tetrahedral sites.

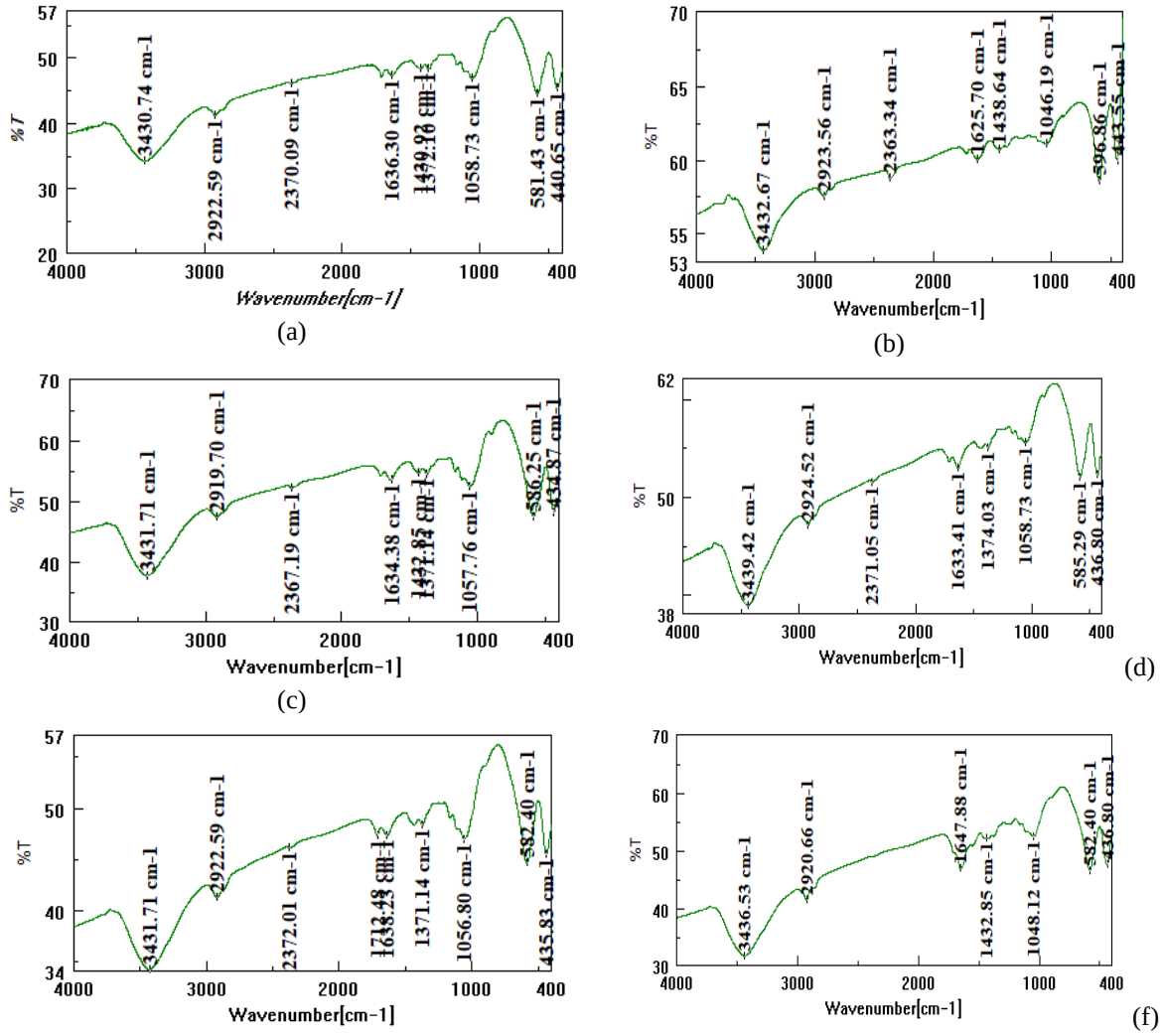

Figure 1. (a,b,c,d,and f) IR pattern $BaNi_{x-2}Zn_xFe_{16}O_{27}$ (x = 0.0 , 0.4, 0.8, 1.2, 1.6 & 2) ferrites. (a) x= 0.0; (b) x=0.4;. (c) x=0 .8; (d) x=1.2; (e) x=1.6; (f) x=2.0.

The alteration in the Fe^{3+}-O^{2-}internuclear distances for the tetrahedral and octahedral sites, respectively, causes the band position change [25,26]. A longer band length is supposed to result in a lower force constantly. The bond length rises if the radius of the impurity ion is greater than the radius of the displaced ion, which lowers the force constant for either site or reduces the repulsive interactions between the ions, resulting in lesser electrostatic energy and, consequently, a lower wavenumber. If a smaller impurity ion takes the place of a metal ion in the normal lattice, the opposite will be accurate. Because zinc has a greater ionic radius (0.74) than the displaced Ni^{2+} ion (0.69), a drop in wavenumber and forces constant is anticipated with zinc replacement [14]. The positions of absorption bands in terms of wavenumber vtet and voct for all samples are summarized in table 1. From Table 1, it is clear that the position of the vtet and voct bands is shifted by incorporating Zn ions in the Ni matrix. The same behavior was reported in previous works on different ferrite systems [27,28]. FT-IR results indicate that Ni ions are stabilized in the O_h crystal field, whereas Zn ions prefer T_d sites because of their ability to form covalent bonds [29-32]. The small shift in band positions for Ba-Zn-Ni ferrites is observed as a function of Zn content (x) (Table 1). It may be caused by differences in the Fe B-O and Fe A-O ionic distances, which are equal to 0.199 nm and 0.189 nm, respectively [33]. This reason can also cause the stronger covalent bonding of Fe^{3+} ions at the tetrahedral sites than at the octahedral sites.

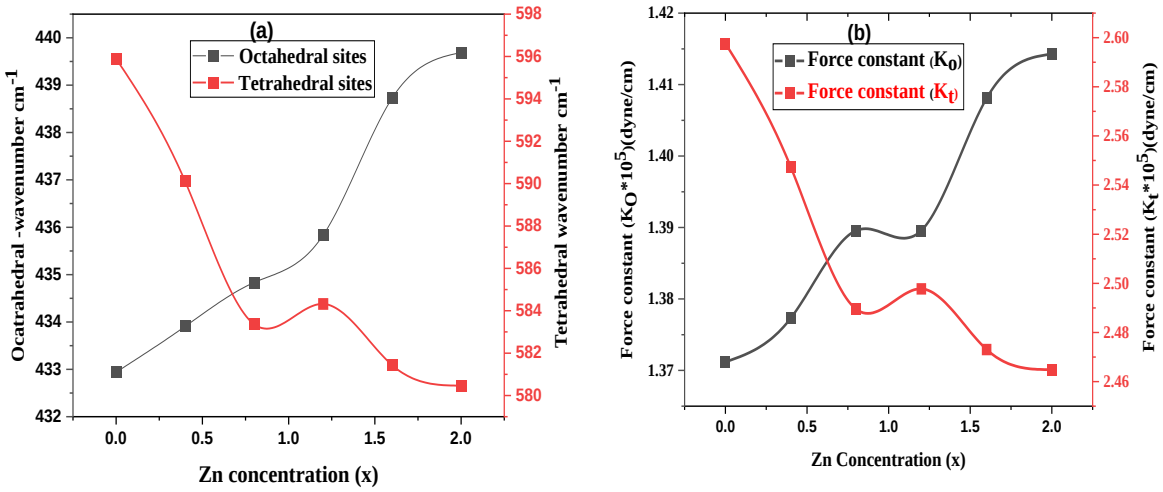

Figure 2. (a)Variation of wave numbers at A and B sites with zinc concentration. (b) force constants with Zinc concentration (x) at the tetrahedral and octahedral sites.

Debye temperature is an essential parameter in studying lattice vibrations [34]. The Debye temperature (θ_D) for $BaNi_{x-2}Zn_xFe_{16}O_{27}$ (x = 0.0, 0.4, 0.8, 1.2, 1.6, and 2) ferrites was obtained by using the next relation [35,36]:

$$\theta_D = \frac{hc\nu_{av}}{K_B}$$

where, c is the speed of light (c = 2.99 10^{10} cm s^{-1}), h is the Plank constant (h = 6.626 10^{-34} J.s), KB is the Boltzmann constant, and v_{av} is the average wave number of bands (cm^{-1}).

Figure 3 and Table 1 contain the computed values for the samples' Debye temperatures (θ_D). It can be noticed that with increasing zinc content, θ_D decreases from 738.19 K (for x = 0.0; to 731.96 K (for x = 1.2), and after those, it remains constant. These values have great importance in determining the conduction mechanism of these ferrites. It can be linked to a decrease in the wavenumber of the peak, usually attributed to Me-O bond vibration in the tetrahedral site. The observed decrease in θ_D (Table 1) with zinc concentration suggests enhancement of the lattice vibrations due to Zn-substitution. It can be seen that θ_D decreases with increasing Zn concentration.

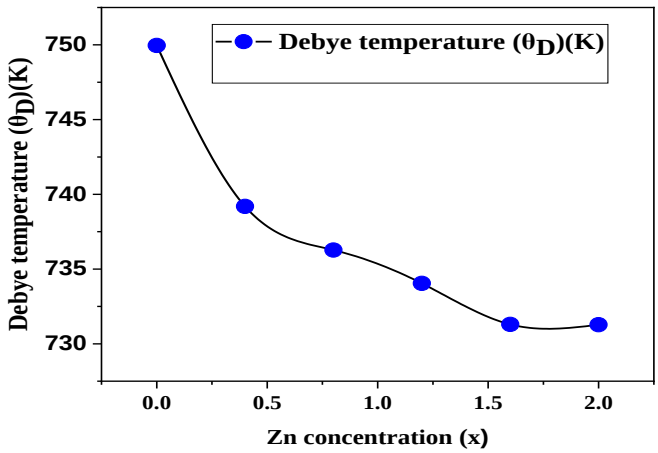

Figure 3. Variation Debye temperature (θ_D)(K)with increasing Zinc concentration (x).

A particular heat theory can be used to discuss these characteristics. This theory states that because some of the heat was absorbed by electrons and D may decrease as Zn concentration increases, conduction in these samples is likely attributable to n-type electrons [37].

Table 1. Calculated force constants of tetrahedral and octahedral sites; Debye temperature.

Composition	**Absorption band (Wave number)**	**Force constants**	**Absorption band (Wave number)**	**Force constants**	**Debye temperature (θ_D)**
x	ν_2 (cm^{-1})	F_{octa} dyn/cm (x 10^5)	ν_1 (cm^{-1})	F_{tet} dyn/cm (x 10^5)	θ_D (K)
X=0	432.94	1.36139	595.896	2.57910	738.1946
X=0.4	433.905	1.36747	590.111	2.52927	734.7363
X=0.8	434.834	1.37333	583.361	2.47174	730.5597
X=1.2	435.834	1.37965	584.325	2.47992	731.9688
X=1.6	438.726	1.39802	581.433	2.45543	731.9688
X=2	439.69	1.40417	580.469	2.44729	731.96888

4. Conclusions

FT-IR spectra of the samples have been analyzed in the frequency range (400-4000) cm^{-1}. The two main bands of absorption corresponding to tetrahedral v_1 and octahedral v_2 were observed, illustrating the ferrite phase formation. The high-frequency band in the range 550-600 cm^{-1} and a low-frequency band at around 400 cm^{-1} were assigned to tetrahedral v_1 and octahedral v_2 sites, respectively. The force constants were calculated for tetrahedral F_{tet} sites and octahedral F_{oct} sites, and frequencies show that K_t decreases with tetrahedral bond length and K_O increases with octahedral bond length. With increasing Zn ions. Debye temperature (θ_D) has also been estimated as a function of composition at room temperature using FTIR spectra. The behavior of debye temperature θ_D showed that electrons should make a significant contribution to the specific heat.

Funding

The research has no external funding.

Acknowledgments

The authors appreciate the contribution of the reviewers in improving the quality of the paper Authors are most grateful **to** the head of the Physics Department at the Faculty of Sciences, Sana'a University -Yemen. Also, the authors are thankful to the UV and FT-IR laboratory team in the Chemistry Department for providing their lab to carry out the present work.

Conflicts of Interest

The authors declare no conflict of interest.

References

1. Dhiman, P.; Jasrotia, R.; Goyal, D.; Mola, G.T. Hexagonal Ferrites, Synthesis, Properties and Their Applications. *Ferrite: Nanostructures with Tunable Properties and Diverse Applications* **2021**, *112*.
2. Bharati, V.A.; Somvanshi, S.B.; Humbe, A.V.; Murumkar, V.D.; Sondur, V.V.; Jadhav, K.M. Influence of trivalent Al–Cr co-substitution on the structural, morphological and Mössbauer properties of nickel ferrite nanoparticles. *Journal of Alloys and Compounds* **2020**, *821*, https://doi.org/10.1016/j.jallcom.2019.153501.
3. Kulkarni, A.B.; Mathad, S.N. Effect of cadmium doping on structural and magnetic studies of Co-Ni ferrites. *Science of Sintering* **2021**, *53*, 407-418.

4. Narang, S.B.; Pubby, K. Nickel Spinel Ferrites: A review. *Journal of Magnetism and Magnetic Materials* **2021**, *519*, https://doi.org/10.1016/j.jmmm.2020.167163.
5. Rehman, A.u.; Shaukat, S.F.; Haidyrah, A.S.; Akhtar, M.N.; Ahmad, M. Synthesis and investigations of structural, magnetic and dielectric properties of Cr-substituted W-type Hexaferrites for high frequency applications. *Journal of Electroceramics* **2021**, *46*, 93-106, https://doi.org/10.1007/s10832-021-00246-7.
6. Batoo, K.M.; Hadi, M.; Verma, R.; Chauhan, A.; Kumar, R.; Singh, M.; Aldossary, O.M. Improved microwave absorption and EMI shielding properties of Ba-doped Co–Zn ferrite. *Ceramics International* **2022**, *48*, 3328-3343, https://doi.org/10.1016/j.ceramint.2021.10.108.
7. Costa, A.C.F.M.; Silva, V.J.; Cornejo, D.R.; Morelli, M.R.; Kiminami, R.H.G.A.; Gama, L. Magnetic and structural properties of NiFe2O4 ferrite nanopowder doped with Zn2+. *Journal of Magnetism and Magnetic Materials* **2008**, *320*, e370-e372, https://doi.org/10.1016/j.jmmm.2008.02.159.
8. Jain, S.R.; Adiga, K.C.; Pai Verneker, V.R. A new approach to thermochemical calculations of condensed fuel-oxidizer mixtures. *Combustion and Flame* **1981**, *40*, 71-79, https://doi.org/10.1016/0010-2180(81)90111-5.
9. Sattibabu, B.; Rao, T.D.; Das, T.; Chatterjee, M.; Bhatnagar, A.K.; Rayaprol, S.; Das, D. Synthesis and magnetic properties of nanostructured Ni1-xZnxFe2O4(x = 0.4, 0.5 and 0.6). *AIP Conference Proceedings* **2020**, *2269*, https://doi.org/10.1063/5.0019566.
10. Tchouank, T.C.T.; Sharma, J.; Mohammed, J.; Kumar, S.; Srivastava, A.K. Effect of temperature on the magnetic properties of nano-sized M-type barium hexagonal ferrites. *AIP Conference Proceedings* **2017**, *1860*, https://doi.org/10.1063/1.4990307.
11. Zhang, C.; Shi, J.; Yang, X.; De, L.; Wang, X. Effects of calcination temperature and solution pH value on the structural and magnetic properties of Ba2Co2Fe12O22 ferrite via EDTA-complexing process. *Materials Chemistry and Physics* **2010**, *123*, 551-556, https://doi.org/10.1016/j.matchemphys.2010.05.013.
12. Ramzan, M.; Arshad, M.I.; Mahmood, K.; Amin, N.; Khan, M.I.; Iqbal, F.; Ajaz-un-Nabi, M. Investigation of Structural and Optical Properties of Pr3+-Substituted M-Type Ba–Ni Nano-Ferrites. *Journal of Superconductivity and Novel Magnetism* **2021**, *34*, 1759-1764, https://doi.org/10.1007/s10948-020-05751-4.
13. Mosleh, Z.; Kameli, P.; Poorbaferani, A.; Ranjbar, M.; Salamati, H. Structural, magnetic and microwave absorption properties of Ce-doped barium hexaferrite. *Journal of Magnetism and Magnetic Materials* **2016**, *397*, 101-107, https://doi.org/10.1016/j.jmmm.2015.08.078.
14. Fatima, N.; Khan, H.M.; Laref, A.; Alhashim, H.H.; Zahid, M.; Nadeem, M.; Akhtar, T.; Anjum, R. Synthesis And Characterization Of Cobalt Substituted W Type Hexagonal Ferrites. *Digest Journal of Nanomaterials & Biostructures (DJNB)* **2021**, *16*.
15. Huang, X.; Zhang, J.; Wang, L.; Zhang, Q. Simple and reproducible preparation of barium hexagonal ferrite by adsorbent combustion method. *Journal of Alloys and Compounds* **2012**, *540*, 137-140, https://doi.org/10.1016/j.jallcom.2012.05.015.
16. da Costa Lima, R.; Pinho, M.S.; Ogasawara, T. Thermal characterization of the intermediary products of the synthesis of Zn-substituted barium hexaferrite. *Journal of Thermal Analysis and Calorimetry* **2009**, *97*, 131, https://doi.org/10.1007/s10973-009-0256-4.
17. Simonescu, C.M.; Tătăruș, A.; Culiță, D.C.; Stănică, N.; Butoi, B.; Kuncser, A. Facile Synthesis of Cobalt Ferrite (CoFe2O4) Nanoparticles in the Presence of Sodium Bis (2-ethyl-hexyl) Sulfosuccinate and Their Application in Dyes Removal from Single and Binary Aqueous Solutions. *Nanomaterials* **2021**, *11*, https://doi.org/10.3390/nano11113128.
18. Davarpanah, E.; Armandi, M.; Hernández, S.; Fino, D.; Arletti, R.; Bensaid, S.; Piumetti, M. CO2 capture on natural zeolite clinoptilolite: Effect of temperature and role of the adsorption sites. *Journal of Environmental Management* **2020**, *275*, https://doi.org/10.1016/j.jenvman.2020.111229.
19. Barbe, A.; Mikhailenko, S.; Starikova, E.; Tyuterev, V. Infrared spectra of 16O3 in the 900 - 5600 cm−1 range revisited: Empirical corrections to the S&MPO and HITRAN2020 line lists. *Journal of Quantitative Spectroscopy and Radiative Transfer* **2021**, *276*, https://doi.org/10.1016/j.jqsrt.2021.107936.
20. Chavan, V.C.; Shirsath, S.E.; Mane, M.L.; Kadam, R.H.; More, S.S. Transformation of hexagonal to mixed spinel crystal structure and magnetic properties of Co2+ substituted BaFe12O19. *Journal of Magnetism and Magnetic Materials* **2016**, *398*, 32-37, https://doi.org/10.1016/j.jmmm.2015.09.002.
21. Balavijayalakshmi, J.; Suriyanarayanan, N.; Jayaprakash, R. Effects of sintering on structural and magnetic properties of Cu substituted cobalt–nickel mixed ferrite nano particles. *Journal of Magnetism and Magnetic Materials* **2014**, *362*, 135-140, https://doi.org/10.1016/j.jmmm.2014.03.005.
22. Raje Shaikh, B.B.; Chishty, S.Q. Auto-ignition synthesis of rare-earth metal-doped Ni–Zn spinel ferrites for electronic applications. *Journal of Materials Science: Materials in Electronics* **2021**, *32*, 23999-24010, https://doi.org/10.1007/s10854-021-06863-w.
23. Chacko, B.; Roy, A.; Melbin Richard, A.; Swathy, J.; Avanish, B.T.; Madhuri, W. Bismuth modified zinc ferrites for low-temperature ceramic co-firing technology. *Materials Chemistry and Physics* **2022**, *276*, https://doi.org/10.1016/j.matchemphys.2021.125401.
24. Ladgaonkar, B.P.; Kolekar, C.B.; Vaingankar, A.S. Infrared absorption spectroscopic study of Nd3+ substituted Zn-Mg ferrites. *Bulletin of Materials Science* **2002**, *25*, 351-354, https://doi.org/10.1007/BF02704131.

25. Shannon, R.D. Revised effective ionic radii and systematic studies of interatomic distances in halides and chalcogenides. *Acta Crystallographica Section A* **1976**, *32*, 751-767, https://doi.org/10.1107/S0567739476001551.
26. Warhate, V.V.; Badwaik, D.S.; Chopne, S.R. Thermal and infrared spectral analysis of TiCo doped NiZn Y-type strontium hexaferrite synthesized by sol gel auto-combustion. *Materials Today: Proceedings* **2020**, *29*, 1055-1058, https://doi.org/10.1016/j.matpr.2020.04.712.
27. Abu-Elsaad, N.I.; Nawara, A.S.; Mazen, S.A. Synthesis, structural characterization, and magnetic properties of Ni–Zn nanoferrites substituted with different metal ions (Mn2+, Co2+, and Cu2+). *Journal of Physics and Chemistry of Solids* **2020**, *146*, https://doi.org/10.1016/j.jpcs.2020.109620.
28. Abul-Magd, A.A.; Morshidy, H.Y.; Abdel-Ghany, A.M. The role of NiO on the structural and optical properties of sodium zinc borate glasses. *Optical Materials* **2020**, *109*, https://doi.org/10.1016/j.optmat.2020.110301.
29. Dawoud, H.A.; Abu Ouda, L.S.; Shaat, S.K. FT-IR studies of nickel substituted polycrystalline zinc spinel ferrites for structural and vibrational investigations. *Chemical Science Transactions* **2017**, *6*.
30. Aly, K.I.; Sayed, M.M.; Mohamed, M.G.; Kuo, S.W.; Younis, O. A facile synthetic route and dual function of network luminescent porous polyester and copolyester containing porphyrin moiety for metal ions sensor and dyes adsorption. *Microporous and Mesoporous Materials* **2020**, *298*, https://doi.org/10.1016/j.micromeso.2020.110063.
31. Venkataraju, C.; Paulsingh, R. FTIR and EPR Studies of Nickel Substituted Nanostructured Mn Zn Ferrite. *Journal of Nanoscience* **2014**, *2014*, 1-5, https://doi.org/10.1155/2014/815385.
32. Kargar, H.; Behjatmanesh-Ardakani, R.; Torabi, V.; Sarvian, A.; Kazemi, Z.; Chavoshpour-Natanzi, Z.; Mirkhani, V.; Sahraei, A.; Nawaz Tahir, M.; Ashfaq, M. Novel copper(II) and zinc(II) complexes of halogenated bidentate N,O-donor Schiff base ligands: Synthesis, characterization, crystal structures, DNA binding, molecular docking, DFT and TD-DFT computational studies. *Inorganica Chimica Acta* **2021**, *514*, https://doi.org/10.1016/j.ica.2020.120004.
33. Ardit, M.; Zanelli, C.; Conte, S.; Molinari, C.; Cruciani, G.; Dondi, M. Ceramisation of hazardous elements: Benefits and pitfalls of the inertisation through silicate ceramics. *Journal of Hazardous Materials* **2022**, *423*, https://doi.org/10.1016/j.jhazmat.2021.126851.
34. Modi, K.B.; Raval, P.Y.; Shah, S.J.; Kathad, C.R.; Dulera, S.V.; Popat, M.V.; Zankat, K.B.; Saija, K.G.; Pathak, T.K.; Vasoya, N.H.; Lakhani, V.K.; Chandra, U.; Jha, P.K. Raman and Mossbauer Spectroscopy and X-ray Diffractometry Studies on Quenched Copper–Ferri–Aluminates. *Inorganic Chemistry* **2015**, *54*, 1543-1555, https://doi.org/10.1021/ic502497a.
35. Tatarchuk, T.; Bououdina, M.; Macyk, W.; Shyichuk, O.; Paliychuk, N.; Yaremiy, I.; Al-Najar, B.; Pacia, M. Structural, Optical, and Magnetic Properties of Zn-Doped CoFe2O4 Nanoparticles. *Nanoscale Research Letters* **2017**, *12*, 141–151, https://doi.org/10.1186/s11671-017-1899-x.
36. Tatarchuk, T.R.; Paliychuk, N.D.; Bououdina, M.; Al-Najar, B.; Pacia, M.; Macyk, W.; Shyichuk, A. Effect of cobalt substitution on structural, elastic, magnetic and optical properties of zinc ferrite nanoparticles. *Journal of Alloys and Compounds* **2018**, *731*, 1256-1266, https://doi.org/10.1016/j.jallcom.2017.10.103.
37. Gamal, W.M.; El-Bassuony, A.A.H.; Abdelsalam, H.K.; Wahab, S.M.A.E. Role of elastic and optical properties on silver nanoferrite and nanochromite for optical switch device applications. *Journal of Materials Science: Materials in Electronics* **2021**, *32*, 21590-21602, https://doi.org/10.1007/s10854-021-06667-y.